Impact of D_2O/H_2O Solvent Exchange on the Emission of HgTe and CdTe Quantum Dots: Polaron and Energy Transfer Effects

Qiannan Wen,[†] Stephen V. Kershaw,*[†] Sergii Kalytchuk,[†] Olga Zhovtiuk,[†] Claas Reckmeier,[†] Mikhail I. Vasilevskiy*[†‡] and Andrey L. Rogach[†]

[†]*Department of Physics and Materials Science and Centre for Functional Photonics (CFP), City University of Hong Kong, Hong Kong S.A.R.*

[‡]*Centro de Fisica, Universidade do Minho, Campus de Gualtar, Braga 4710-057, Portugal*

Corresponding authors: skershaw@cityu.edu.hk (SVK), mikhail@fisica.uminho.pt (MIV)

Abstract

We have studied light emission kinetics and analyzed carrier recombination channels in HgTe quantum dots that were initially grown in H_2O. Replacing the solvent by D_2O, the non-radiative recombination rate changes highlight the role of the vibrational degrees of freedom in the medium surrounding the dots, including both solvent and ligands. The contributing energy loss mechanisms have been evaluated by developing quantitative models for the non-radiative recombination via (i) polaron states formed by strong coupling of ligand vibration modes to a surface trap state (non-resonant channel) and (ii) resonant energy transfer to vibration modes in the solvent. We conclude that channel (i) is more important than (ii) for HgTe dots in either solution. When some of these modes are removed from the relevant spectral range by the H_2O to D_2O replacement, the polaron effect becomes weaker and the non-radiative lifetime increases. Comparisons with CdTe quantum dots (QDs) served as a reference where the resonant energy loss (ii) *a priori* was not a factor, also confirmed by our experiments. The solvent exchange (H_2O to D_2O), however, is found to slightly increase the overall quantum yield of CdTe QD samples, probably by increasing the fraction of bright QDs in the ensemble. The fundamental study reported here can serve as the foundation for the design and optimization principles of narrow bandgap quantum dots aimed at applications in long wavelength colloidal materials for infrared light emitting diodes and photodetectors.

Introduction

Colloidal semiconductor quantum dots (QDs) are low-cost and easily processed materials for applications in photodetectors, solar cells, light emitting diodes, etc.[1-6] Understanding the carrier decay mechanisms in QDs is of particular importance in order to improve both the basic QD materials and heterostructure designs so as to enhance the device performance. The interplay between radiative and non-radiative recombination processes determines the overall photoluminescence (PL) quantum yield (QY) of QD materials. While the radiative recombination of a QD is largely dependent on the intrinsic properties determined by the QD material and quantum confinement effects influenced by its immediate surroundings, the synthetic conditions, post-synthetic treatment and the macroscopic environment (solvent, substrate etc.) can have a major impact upon the non-radiative rate. The aim of this work is to get insight into the capabilities of the surface chemistry to control the IR light emission properties of HgTe QDs by exploiting relevant physical mechanisms influenced by the ligand and solvent environment close to the surface of the dots. QD interactions between the solvent and ligand are strong and have a very substantial impact in the mid-IR (e.g. beyond 3000 nm) where vibrational modes of molecules have large oscillator strengths (fundamental mode or low overtone and combination (OTC) modes) and QD PLQYs are low. However, even at shorter NIR wavelengths where QD PLQYs are higher, strong OTCs in aqueous solutions can still have a substantial effect on QD emission spectra. This paper investigates the QD interactions with the local molecular environment at NIR wavelengths where detailed PL and lifetime measurements are still relatively straightforward to make, but which have not hitherto been explored in terms of the fundamental coupling mechanisms of which there may be several operating in competition.

The radiative rate in colloidal QDs of II-VI materials is determined by dipole-allowed low-energy exciton transitions and the structure of involved exciton states is well understood for wide gap materials. For HgTe QDs, there is a difficulty coming from the peculiar band structure of this material near the Γ point. Nevertheless, tight-binding calculations provide a good quantitative description of the size-dependent exciton states and absorption spectra of nearly spherical HgTe nanocrystals.[7,8] The non-radiative decay mechanisms that have been proposed in the literature vary among the types of materials, the surface conditions etc.[7-10] Carriers trap at QD surface states, and a frequently reported related mechanism in CdTe, CdSe, PbS QDs involves complex transition modes.[9-11] Califano[10] proposed recently that for CdTe QDs two types of unsaturated bonds at Te surface atoms lead to distinct relaxation time scales and sensitivities to the surrounding environment. Surface states have not been extensively characterized for IR emitting HgTe QDs yet. Much of the recent insight into the carrier dynamics of the wider bandgap QD materials centered on such surface states has been derived from single dot spectroscopy and fs pump-probe spectroscopy,[12] which are far easier and the equipment less expensive to build for visible and near IR operating wavelengths. Some work has already been done on narrow bandgap QDs, for example, resonant coupling between electronic states of HgTe QDs to the vibrational states of the ligands was suggested by Keuleyan et al.[13] to be the major non-radiative decay mechanism at long wavelengths spanning the hydrocarbon vibrational bands. Most of the studies on long wavelength emitting HgTe QDs focus on the interaction between different chemical states arising from the ligand, surface

treatments and temperature changes, while the physical interactions at the QD surface possibly are overlooked.

Here we present the results of D_2O/H_2O solvent exchange of colloidal CdTe and HgTe QDs. This method has the advantage of decoupling the physical interactions between the QD surface and the surrounding medium without other chemical changes. Emission decay rate is affected by the surrounding medium in two ways: (i) change of the radiative lifetime (by changing the refractive index and its dispersion, which affects the photon density of states), and (ii) non-radiative losses (when the exciton energy is irreversibly transferred to some other excitations and finally is dissipated into heat). We find that the solvent replacement affects both radiative and non-radiative decay rates of HgTe QDs yielding a higher quantum yield and a longer photoluminescence lifetime for the same dots dissolved in heavy water. The emission from CdTe QDs is in the visible and far away from any IR vibrational modes in either solvents or ligands. It thus serves as a reference for the HgTe QDs which do emit in the overtone and combination (OTC) band range of the solvents and ligands. Still, we have found that the PL lifetime and the QY both increase by some 10% with the solvent exchange ($H_2O \rightarrow D_2O$), probably caused by an increase of the fraction of bright QDs in the ensemble. As far as HgTe QDs are concerned, we found that the observed changes in the decay rates cannot be accounted for only by resonant energy transfer to vibration modes in the solvent. These findings imply that the isotopic replacement's effect is not limited to the most obvious change of the molecular vibration frequencies. We used a relatively gentle transfer method (freeze drying) rather than precipitation to switch between the two solvents, so that QD-ligand binding is not significantly disturbed, allowing us to isolate changes that are specifically connected with the solvent environment. Moreover, since the solvents chosen, H_2O and D_2O, are chemically quite similar, it limits the range of physical mechanisms that may be affected by the replacement. We discuss our experimental findings in terms of strong coupling of ligand vibration modes to a surface trap state and resonant energy transfer to vibration modes in the solvent, which provide efficient non-radiative recombination mechanisms in low bandgap QDs. We also speculate how the solvent replacement can affect the radiative lifetime in HgTe QDs.

Experimental section

Chemicals

Mercury perchlorate hydrate ($Hg(ClO_4)_2 \cdot xH_2O$), 1-thiolglycerol (TG), mercaptopropionic acid (MPA), and toluene from Sigma-Aldrich were used in syntheses and phase transfer. Milli-Q deionized water (H_2O) and deuterium oxide (D_2O 99.9% D, from Sigma-Aldrich) were used in solvent exchange.

Syntheses of CdTe and HgTe QDs

The CdTe QDs used in this experiment were synthesized in aqueous solution with MPA as a ligand according to the method reported by Wu et al.[14] As-synthesized materials were 5 times diluted and heat treated with a small addition of sodium bicarbonate (5g/500ml) for 30min at 80°C so that the clusters formed during the initial synthesis were broken apart and QDs emission properties were enhanced[15, 16]. Aqueous based HgTe QDs were synthesized at room temperature using the method previously reported.[17, 18] Typically, 160ml of deionized water (H_2O) in the main

reaction flask was degassed using argon for an hour, and then 72ul (0.67mmol) of TG added. The pH was adjusted to 10.8, followed by addition of 127mg (0.32mmol) of $Hg(ClO_4)_2$ dissolved in 10 ml of neutral H_2O. H_2Te gas was generated in an electrolysis cell with phosphoric acid (typically 60% concentrated) as electrolyte, platinum wire as the anode and a custom made tellurium cathode. The gas, buffered in a slow continuous flow of Ar, was passed over into the solution in the main reaction flask via a tube. The flow of H_2Te gas was stopped when the PL peak reached 1000nm. Increasing the concentration of metal precursor by a factor of 1.5 helps to stabilize the size distribution of small HgTe QDs (diameter around 3 nm in this experiment), but the size and PL peak position still slowly drift (towards larger diameter and wavelength) over the course of the following few weeks. The rate of post-synthetic growth decreases exponentially so the first samples were taken 1 day after synthesis so that PL drift becomes reasonably slow on experimental timescales. However, allowing the solution to stand for several further days allowed more samples to be taken at still longer PL wavelengths, effectively scanning the emission over ligand and solvent vibrational OTC bands.

<u>D_2O/H_2O solvent exchange of CdTe and HgTe QDs</u>

To switch the solvent from H_2O to the isotopically heavier D_2O, samples of as-synthesized CdTe and HgTe QDs in water were freeze dried in vacuum for one day and then re-dissolved in D_2O. A reference sample for each was processed in the same way but simply dissolved in H_2O after freeze drying in order to assess any impact of the freeze drying process itself. After measurement, the two resulting samples were freeze dried again and each dissolved in the other solvent (i.e. 'crossed-over' so D_2O solutions become H_2O solutions and *vice versa*). Measurements were repeated to check if QDs change or recover without significant difference after solvent cross-overs. Table 1 shows the solvent exchange procedure for two samples (**a** and **b**) for each type of QDs.

Table 1 The solvent exchange procedure for CdTe and HgTe QDs. All samples were fully dried in vacuum before they were re-dissolved in the solvent. The freeze drying cycle can be repeated many times without sample degradation.

		1st solvent		2nd solvent
CdTe in H_2O		**a.** D_2O		**a.** H_2O
	Dried →	**b.** H_2O	Dried →	**b.** D_2O
HgTe in H_2O		**a.** D_2O		**a.** H_2O
		b. H_2O		**b.** D_2O

<u>Spectroscopic measurements</u>

PL spectra were measured on an Edinburgh Instruments FLS920P spectrometer system. The PL spectra and decay curves of CdTe QDs were measured using a photomultiplier tube (PMT) covering the visible and NIR range to 830 nm (Hamamatsu R 928). HgTe QDs emitting in the NIR were measured with an InP/InGaAs PMT cooled by the vapor from liquid nitrogen (-80 °C), with a xenon lamp and excitation monochromator set at 405 nm. For time-resolved PL measurements, a pulsed

diode laser with emission wavelength at 405 nm in conjunction with a Time Correlated Single Photon Counting (TCSPC) system was used for both CdTe and HgTe QDs. In these measurements the time scale was set at 500 ns to record the full PL decay under the same conditions. PL QYs for all samples were measured using an integrating sphere, under cw excitation. The xenon lamp set at 405 nm was used as excitation source for CdTe and the amplified spontaneous emission from a 2W 880 nm laser operated below threshold was used for HgTe QDs. Absorption spectra of all samples were measured on a Shimadzu UV 3600 UV/ visible/ IR spectrometer. The hydrodynamic size of the HgTe QDs was measured using a Malvern Instruments dynamic light scattering (DLS) machine to ensure that particle aggregation had not occurred during the synthesis or after the freeze drying/ re-dissolution processes.

Results and discussion

Absorption and emission spectra

Figures 1 (a) and (b) show the absorption and PL spectra for CdTe and HgTe QDs dissolved in H_2O and D_2O. Samples are diluted in 1cm path length cuvettes for absorption measurements and narrower cuvettes (orthogonal emission and excitation with approximately 1mm path length for the emission in the direction of the detector) for PL studies. CdTe QDs emitting at around 640nm show a slight decrease of PL intensity for the sample in H_2O compared with that for D_2O. Absorption spectra normalized at 405nm nearly overlap for H_2O and D_2O solutions, but the PL of HgTe QDs is strongly quenched in H_2O. Figure 1 (c) shows the absorbance of H_2O and D_2O (1cm path length) from the visible to NIR as measured. The combined stretching and bending modes of water molecule vibrations constitute the absorption bands in the NIR,[19] the frequencies of which are shifted upon isotopic replacement of H by D in the solvent. The oscillator strengths of the respective vibrational bands are also lowered slightly in D_2O. The effect of simple solvent attenuation (i.e. the signal reduction if water behaved simply as an optical filter with no direct interaction with the emission process in the QDs) can be assessed by taking the emission in D_2O and scaling it according to the H_2O and D_2O absorbance difference. This simple passive effect would slightly lower the PL intensity on going from D_2O to H_2O as represented by the dotted line in figure 1 (b). However, this solvent-absorption corrected spectrum highly exceeds the measured PL intensity in H_2O shown by the green line. Passive solvent absorption is too weak to account for such a large PL quench in the vicinity of the H_2O $\nu_1 + \nu_2 + \nu_3$ combination band. Both HgTe and CdTe QD sample measurements were repeated after a further solvent cross-over, and similar results were obtained as for the first run. There is little surface damage seen in the process of freeze drying, where QDs are re-dissolved easily forming a stable solution each time. Compared with other drying methods such as heating and precipitation which would either introduces more surface defects or disturb the size distribution of the QDs, freeze drying preserves the original size of the QDs and the TG ligand coating remains intact.

PL decay kinetics

Figure 2 shows the PL decay curves for CdTe QDs (a,b) and HgTe QDs (c,d). Both samples are

recorded for their PL decays at three wavelengths: one centered at the PL peak and two others on either side of the peak. The decay curves for QDs dissolved in D_2O show less wavelength dispersion. Insets are the PL decays of QDs in two solvents at the PL peak wavelength, showing a faster decay in H_2O for both samples. In order to characterize PL decay curves in a way that would be free from any *a priori* model, we evaluated average (effective) PL lifetimes (τ_{avg}), from the experimental PL kinetics [$I(t)$] by using the equation[20]:

$$\tau_{avg} = \frac{1}{I(0)} \int_0^\infty I(t)dt \, , \tag{1}$$

where the integration was performed numerically. Table 2 lists the average PL lifetimes obtained by Eq. (1) and measured PL QYs.

Table 2 Average lifetimes for time-resolved PL decays of CdTe and HgTe QDs at PL peak wavelengths, calculated by Eq. (1), and steady state PL quantum yields.

	λ	Solvent	τ_{avg} (ns)	PL QY (%)
CdTe	640nm	H_2O	24.4	77
		D_2O	26.9	86
HgTe	1065nm	H_2O	49.5	5
	1058nm	D_2O	89.2	20

From the average PL lifetime and overall (measured) QY, the radiative and non-radiative components in the total PL decay for an ideal system of identical QDs could be obtained through the relations:
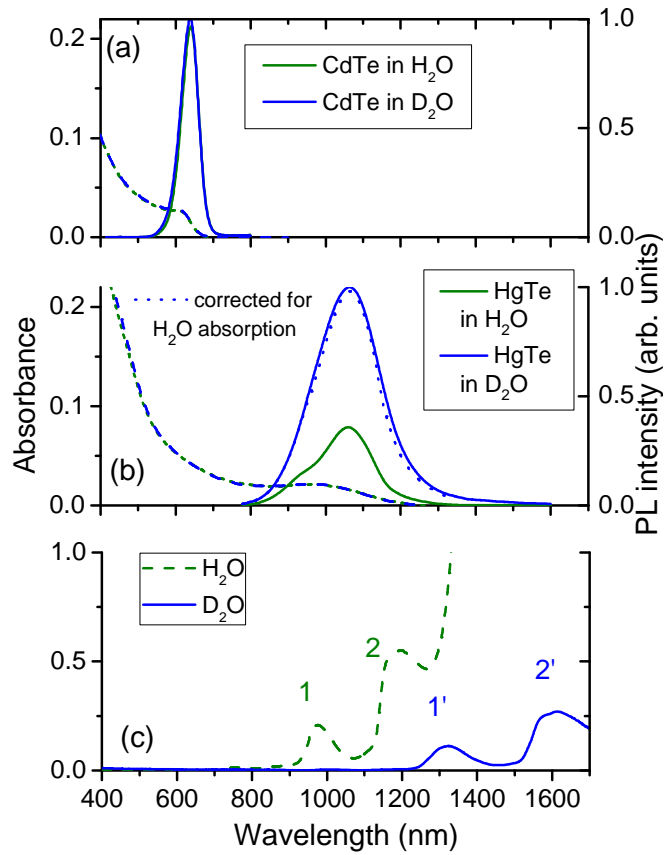
$$\tau_r = \tau_{avg} / QY \, , \tag{2}$$

Figure 1. Absorption and PL spectra for: (a) CdTe and (b) HgTe QDs, in H_2O and D_2O. The same concentration is kept for each sample in the two solvents. The dotted line in (b) is the estimated PL spectrum for HgTe QDs in H_2O based on the emission spectrum for HgTe in D_2O and the absorbance difference between pure H_2O and D_2O. The solvents' absorption spectra are shown in (c) where several combination bands of molecular vibrations are labelled: $2\nu_1 + \nu_3$ (1 for H_2O and 1' for D_2O), $\nu_1 + \nu_2 + \nu_3$ (2 for H_2O and 2' for D_2O). Here ν_1, ν_2 and ν_3 are the frequencies of symmetrical stretching, bending and asymmetrical stretching modes for H_2O (fundamentals at 3261 cm^{-1}, 1639 cm^{-1}, 3351 cm^{-1}) and D_2O (fundamentals at 2407 cm^{-1}, 1206 cm^{-1}, 2476 cm^{-1}), respectively. The solvent's absorption was subtracted in (a) and (b).
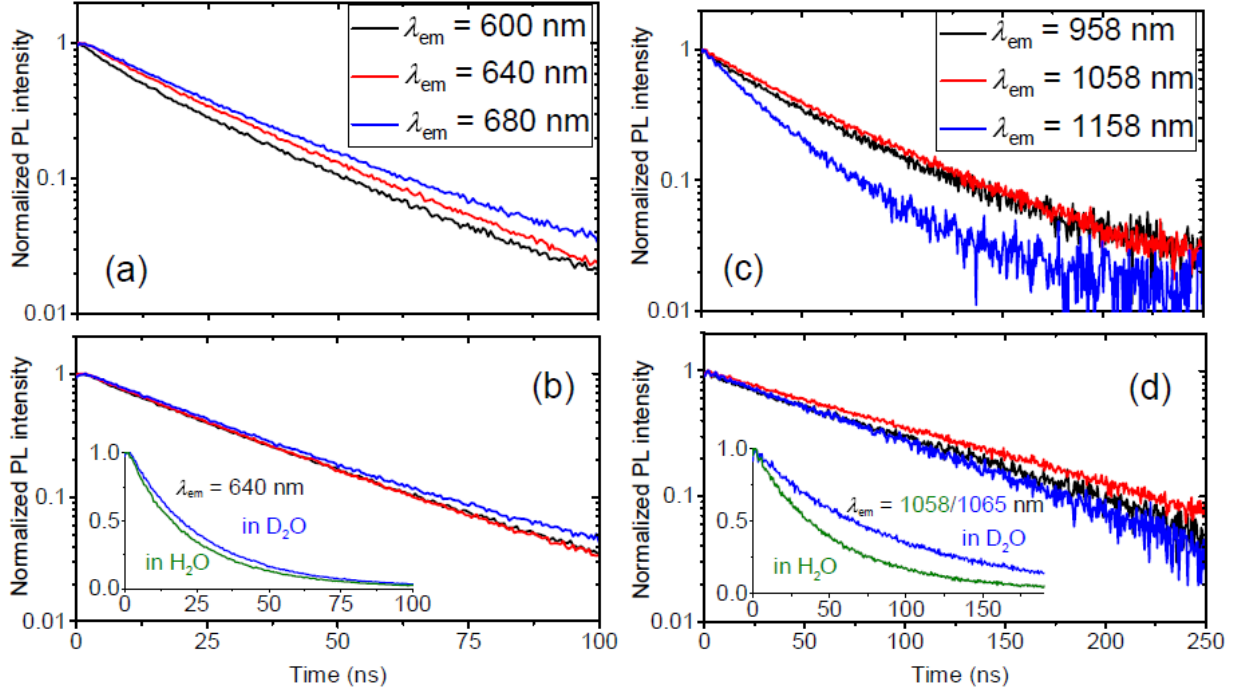
Figure 2. PL decays (shown in logarithmic scale) measured at different emission wavelengths as indicated on frames for CdTe QDs in H_2O (a) and D_2O (b); for HgTe QDs in H_2O (c) and D_2O (d). Insets are PL decay comparisons for each sample at its PL peak (CdTe at 640 nm and HgTe at 1058 nm, linear scale).

$$\tau_{nr} = \tau_{avg}/(1-QY), \qquad (3)$$

where τ_r and τ_{nr} are the radiative and non-radiative lifetimes, respectively. However, eqs. (2) and (3) ignore the presence of dark (not emitting) dots, which is known to be an important issue for colloidal QDs.[21-23] We considered corrections to these equations taking a simple model assuming the presence of a certain fraction of dark particles having very large non-radiative rates (while the oscillator strength of the optical transition is the same for all dots). The details are presented in Supplementary Material (SM). Our conclusion is that eq. (2) is exact, while eq. (3) overestimates the non-radiative recombination rate. As shown in the SM, if the fraction of bright dots is $p < 1$ and the remaining particles are completely dark because of the very fast non-radiative decay, eq. (3) needs to be corrected as follows:

$$\tau_{nr} = \frac{\tau_{avg}}{1-QY}f_{cor}(p,QY); \qquad f_{cor}(p,QY) = \frac{1-p\cdot QY}{p(1-QY)} \quad . \qquad (4)$$

The correction function in eq. (4), $f_{cor}(p,QY) \geq 1$, becomes increasingly important as the fraction of

"dark" QDs $(1-p)$ increases. For instance, $\left(f_{cor}-1\right)$ can reach ~25 % for $QY=0.2$ and > 50 %

for $QY=0.8$ when some 20% of the dots are completely silent, a realistic value according to the

experimental data of Refs.[21,22] On the other hand, for low QY values, its dependence on the fraction

of dark/bright QDs is rather weak (see SM), which means that relative changes (not the absolute

values) of the non-radiative decay time between samples with fixed p can be estimated even
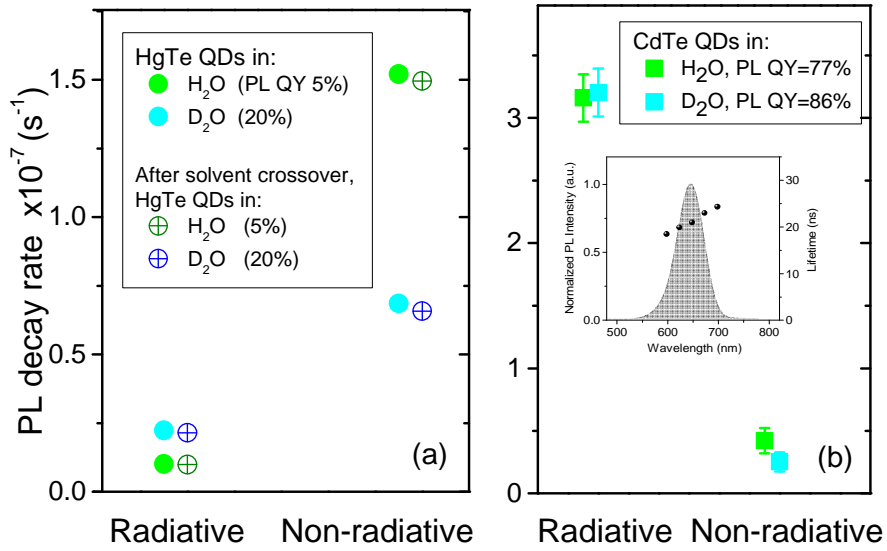
using eq. (3).

Figure 3. Radiative and non-radiative rates for CdTe (a) and HgTe (b) QDs in different solvents. Otherwise overlapping points are offset for clarity. In most of the cases error bars are smaller than the symbol size. The inset in (b) shows the wavelength dependence of PL lifetimes measured across the emission spectrum profile of the CdTe QDs.

Figure 3 shows the radiative and non-radiative decay rates (the inverse of the corresponding

lifetime) for CdTe and HgTe QDs in different solvents calculated by eqs. (2) and (4) using input data

from Table 2. For highly luminescent CdTe QDs we estimated $p \approx QY$, while for HgTe dots we

assumed p=0.8. The plot summarizes the main experimental findings of this work and shows that the observed changes are reproduced after alternated exchanges of the solvent. Their explanation will be presented in the following section. Here we just notice that the obtained radiative recombination rate for CdTe dots is consistent with the known data from the literature, namely, the raidative lifetime of CdTe QDs of similar size ≈30 ns.[24,25]
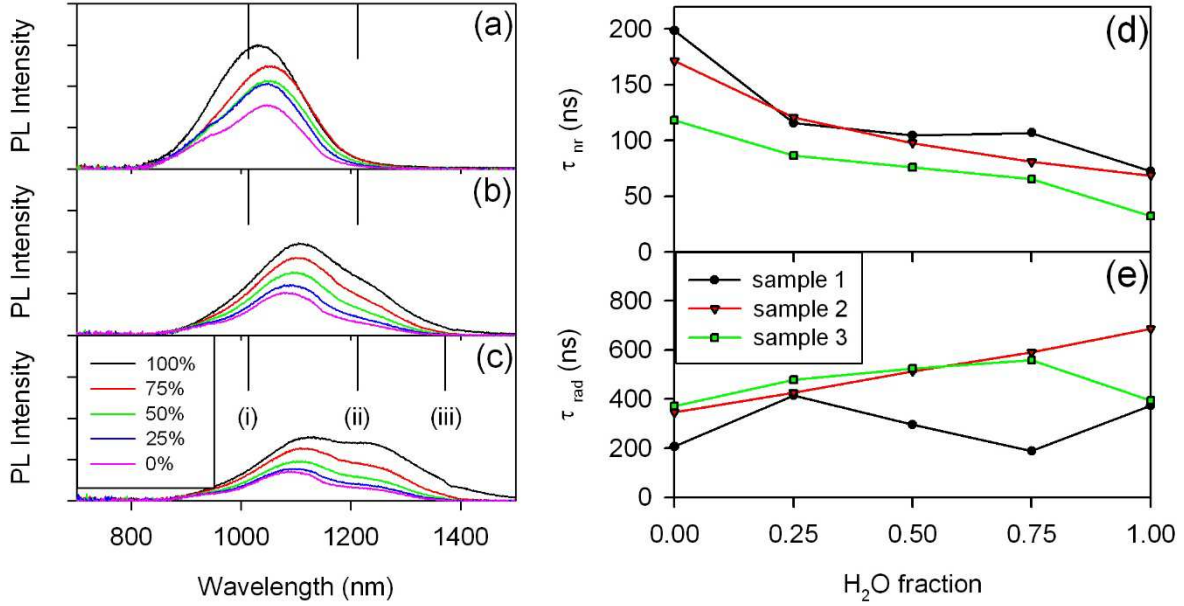
Figure 4. (Left panels) PL spectra for HgTe QD samples 1 (a), 2 (b) and 3 (c) in mixed H_2O/D_2O solutions. Volume fractions of D_2O are shown in the inset to (c). Also indicated in panel (c) are the nominal peak wavelengths for the combination bands of H_2O, D_2O: (i) $2v_1 + v_3$ H_2O; (ii) $v_1 + v_2 + v_3$ H_2O; (iii) $2 v_1 + v_3$ D_2O). (Right panels) (d) Non-radiative and (e) radiative lifetimes in mixed H_2O/D_2O solvents evaluated at the PL peak wavelength for samples 1 and 2, and at 1208 nm (midway between the apparent double peaks) for sample 3.

Further measurements of PL spectra, PL QYs and lifetimes of HgTe QDs were made on solutions with mixed H_2O/D_2O compositions. Aliquots from the synthesis solution were taken after the stop of telluride gas flow on day 1 (sample 1) and on leaving the main growth solution to stand and shift slowly to longer wavelengths for 3 days (sample 2) and 5 days (sample 3). In this manner the relatively broad PL emission could be tuned slowly across the H_2O $v_1 + v_2 + v_3$ and $2v_1 + v_3$ combination bands. As before, the solutions were freeze dried to remove the aqueous solvent and then re-diluted in H_2O/D_2O mixed solvents at volume fractions of 0%, 25%, 50%, 75% and 100%. The respective PL spectra of these solutions are shown in figure 4 and the relevant solvent OTC bands are marked for reference (the full solvent absorption spectra are also shown in figure 1 (d)).

The PL QYs and average decay times were measured for each of the solutions and based on these measurements, radiative and non-radiative lifetimes were extracted as also shown in figure 4. Whilst the PL QY (not shown) for each of the three samples falls monotonically with increasing H_2O content, and the non-radiative lifetimes likewise show the same trend (fig. 4d), the radiative lifetime (fig. 4e) behavior is a little less straightforward. For sample 3 which has the biggest overlap with the H_2O $v_1 + v_2 + v_3$ combination band, the impact on the non-radiative lifetimes is strongest, with an increase in the rate of 30-50%. The biggest impact on the radiative rate is for sample 2, which is intermediate between samples 1 and 3 in terms of superposition of its PL band with the

$v_1 + v_2 + v_3$ and $2v_1 + v_3$ bands of water, so it is hard to see here any clear correlation between the spectral overlap and the radiative lifetime.
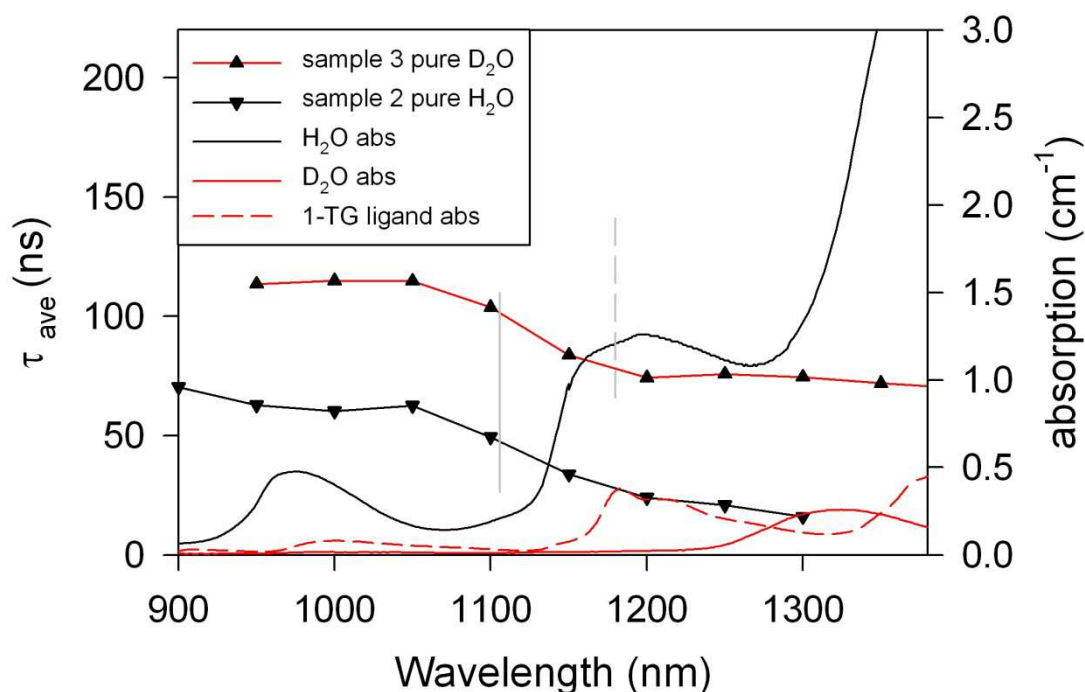

Figure 5. Average decay lifetimes measured at different wavelengths across the PL spectrum for sample 2 in pure H_2O and for sample 3 in pure D_2O. The grey vertical lines indicate the PL peak positions (see Fig. 4). The absorption spectra of pure H_2O, D_2O and the TG ligand are shown for reference.

In order to gain a spectral insight concerning the observed changes in the decay rates, we also measured the average PL decay times at a number of wavelengths across the emission peaks for a pair of D_2O and H_2O samples as shown in figure 5. Since the spectral dependence of the PL QY is not known, we just present the average decay times, though the relatively low integrated QY values for HgTe QDs suggest that the total decay rate is dominated by the non-radiative contribution. The peak PL wavelengths for each sample are indicated by the vertical grey lines and the solvent and ligand IR absorption spectra are also shown alongside the lifetime spectra. For sample 2 where the emission spans two H_2O absorption peaks (around 1000 nm and 1200 nm), there are matching dips in the average lifetimes, which probably indicate faster non-radiative decay rates. For sample 3 there is a still noticeable dip in the average lifetime around 1200 nm, even though there is virtually no D_2O solvent absorption around this region. However, the ligand molecule, TG, still contains a pair of OH groups and also CH groups (where no hydrogen-deuterium replacement occurred), which contribute to the IR absorption in this range. Therefore the QD solution of sample 3 shows some sensitivity (the faster non-radiative rate and a dip in the emission spectrum) around 1200nm despite the use of pure D_2O as solvent. These findings indicate that both surface ligand and solvent

vibrational modes contribute to the QD non-radiative decay in a resonant manner. However, we notice that there is a more substantial global increase in the PL decay time for the whole spectral region studied. Moreover, it shows a moderate general decrease for larger wavelengths, while the opposite tendency is expected from the theory describing radiative decay and has been verified experimentally in the case of CdTe QDs studied here (inset in Figure 3b) for the radiative lifetime. It implies that there must be other energy loss processes (e.g. surface trap mediated non-radiative recombination), which have no resonant dependence upon the emitted photon wavelength. In the next section we propose theoretical models for both resonant and non-resonant non-radiative decay channels in HgTe QDs.

Theoretical model

<u>Non-radiative decay rate</u>

Non-radiative losses in QDs occur *via* two channels: (1) a Förster type resonant energy transfer channel where the exciton energy is irreversibly transferred to some other excitations in the QD's environment and finally is dissipated into heat, and (2) a non-radiative recombination process inside the dots. Let us first concentrate on the latter. Since the energy gap in HgTe QDs studied here is still relatively large, direct non-radiative recombination *via* emission of a large number of phonons is improbable and, as in bulk semiconductors, it is more likely to occur via electron or hole capture into some intermediate state(s) where it would wait for the partner particle to recombine. The existence of traps on the surface of colloidal QDs is well documented and even some microscopic models of them have been proposed.[10] Unlike in bulk semiconductors where the traps involved in non-radiative recombination are located somewhere in the middle of the gap, shallow traps should be more efficient in QDs. It is because the electron or hole capture into a deep surface trap should be hard since the overlap of the wavefunctions corresponding to the QD core and the surface state is small rendering a negligible phonon-assisted transition matrix element between them. Therefore a trap "ideal for recombination" should have a state nearly matching (within a thermal energy, $\approx k_B T$) either electron or hole ground state in the QD core and also possess some other states located deeper in the forbidden band of the dot, which would facilitate the encounter with the partner particle.

It is unlikely that a defect with such an electronic structure may exist on the surface but a sufficiently strong coupling to a discrete vibrational mode (e.g. optical phonon mode of a polar semiconductor or a molecular vibration) can generate a set of levels (phonon replicas) from a single electronic level, as known from the solution of the so called independent boson model[26] yielding a mixed electron-phonon quasiparticle called a polaron. In the simplest version of this model, the polaron energy spectrum consists of equidistant levels spaced by the energy of the single phonon mode considered, $\hbar\omega_0$, and the spectral density of states (SDS) is determined by the ratio between the electron-phonon coupling constant and $\hbar\omega_0$ (the square of this ratio is often called Huang-Rhys parameter, S). However, the strength of coupling to QD optical phonons for the core

state is by far too low (i.e. the Huang-Rhys parameter generalized to include all relevant optical phonon modes is too small, $S \ll 1$)[27, 28] to make it relevant for relaxation from the 1P to the 1S state in wide gap QDs or for recombination in our HgTe dots, which would require S of the order of 10.[27] Another possibility is that the surface trap state is strongly coupled to some vibration modes of ligand molecules, as has been suggested in Ref.[12] Indeed, such a coupling can be very strong and the polaron effect in molecular crystals can be very large compared to semiconductors, for instance, in polyacene crystals it is of the order of 150 meV.[29] It would be sufficient to create polaron states throughout the broad interval of forbidden energies in a QD and such states could act as a staircase for carrier's relaxation and eventual recombination. In principle, owing to the finite confinement barrier, the core electron state also couples to ligand vibrations, as it was suggested in order to explain fast hole relaxation in wider bandgap (CdSe) QDs.[30] However, such a diagonal coupling should be small in our case because of stronger confinement of the electron wavefunction inside the core; in any case, it does not affect the non-adiabaticity (i.e. the phonon-mediated coupling between the core and surface states), which is the most important ingredient in our model.
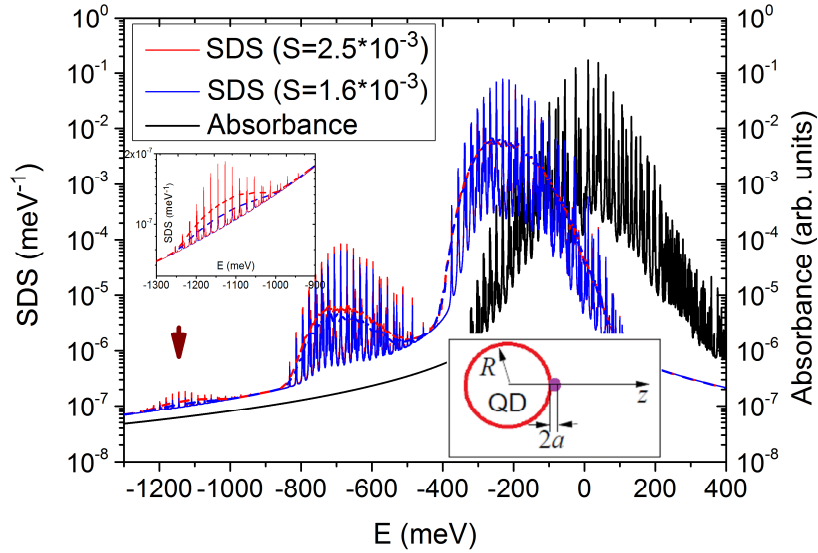

Figure 6. Spectral density of states (SDS) calculated for two bare electron levels separated by $\Delta = 20$ meV and phonon energies given in the text and $G_{12} = 35$ meV. Two values of the Huang-Rhys parameter model the cases of H_2O $\left(S = 2.5 \cdot 10^{-3} \right)$ and D_2O $\left(S = 1.6 \cdot 10^{-3} \right)$ solvents at $T = 300$ K. The absorption spectrum calculated as explained in Ref.[31] is also shown, which is almost identical for both values of S. The arrow indicates the polaron band involved in carrier recombination: smooth curves within this band are guides to the eye. The insets show schematics of our model system and zoom into the energy range relevant for the recombination.

We shall consider the following model of non-radiative recombination in our HgTe QDs:

(i) There is a strongly localized trap state on the QD surface, either slightly below the $1S_e$ electron

state or slightly above the 1S$_{3/2}$ hole state in the QD core. For definitiveness we shall assume the former. The wavefunction of this state will be assumed of the hydrogen-like form (see the inset in Fig. 6):

$$\Psi_t(\mathbf{r}) = (\pi a^3)^{-1/2} \exp\left\{\frac{|\mathbf{r} - (R+a)\mathbf{e}_z|}{a}\right\},$$ (5)

where a is its localization radius and R is the QD radius. This state is connected with the 1S$_e$ state in the QD core because the latter's wavefunction does not vanish at $r = R$ owing to the finite potential barrier at the QD surface,

$$\Psi_{1S}(\mathbf{r}) = \begin{cases} A\sin(kr)/r, & r \leq R \\ bA\exp(-\kappa r)/r, & r \geq R' \end{cases}$$ (6)

where $k^2 = 2mE_{1S}/\hbar^2$, $\kappa^2 = 2m(V_0 - E_{1S})/\hbar^2$ with m being the effective mass and V_0 denoting the potential barrier height, A is a normalization constant and b is a coefficient defined by the continuity conditions at $r = R$. These conditions also determine the energy level, E_{1S}, through the equation

$$\cot(kR) = -\kappa/k.$$ (7)

(ii) The trap and core states are linked *via* interaction with QD optical phonons. These polar modes have an associated electrostatic potential which does not vanish outside the dot for phonons with angular momenta $l_p \geq 1$ (sometimes they are referred to as surface modes although it is more correct to call them coupled longitudinal-transverse-surface modes; those with $l_p = 1, 2$ and 3 have been observed for II-VI QDs by means of FIR[32] and Raman[33] spectroscopy. The importance of the non-diagonal coupling (non-adiabatic effect) has been emphasized in relation with phonon replicas in PL spectra and overtone modes in Raman spectra of QDs.[34, 35]

Considering only the Fröhlich mechanism, the interaction matrix element between the two states is given by

$$g_{12}^\nu = e\int \varphi_\nu(\mathbf{r})\Psi_{1S}(\mathbf{r})\Psi_t(\mathbf{r})d\mathbf{r},$$ (8)

where ν stands for all three indices of the QD phonon mode (l_p, m_p and n_p) and $\varphi_\nu(\mathbf{r})$ denotes the electrostatic potential created by the mode; we shall not reproduce here a rather lengthy expression for it, which can be found in Ref.[28] If we plug the wavefunctions (5) and (6) into

(8), we can obtain the following expression[a]

$$g_{12}^{v} \approx \frac{1}{\sqrt{2\pi}} C_F \left(\frac{a}{R}\right)^{3/2} \left(\frac{E_{1S}}{V_0 - E_{1S}}\right)^{1/2} (2l_p + 1)^{1/2} \Phi_{l_p n_p}(R), \qquad (9)$$

where

$$C_F = e\sqrt{2\pi\hbar\omega_{LO}\left(\varepsilon_\infty^{-1} - \varepsilon_0^{-1}\right)/R}$$

is the Fröhlich constant with $\hbar\omega_{LO}$, ε_∞ and ε_0 denoting the bulk LO phonon energy and the

high-frequency and static dielectric constants, respectively. The function $\Phi_{l_p n_p}$ is given in Ref.[28]

and Eq. (9) holds for $l_p \geq 1$, $m_p = 0$ and arbitrary n_p (otherwise $g_{12}^{v} = 0$). We notice that,

unlike for diagonal matrix elements, it is non-zero for a broad variety of phonon modes because of
the different symmetry of the electronic states involved. It can render strong non-adiabatic effects
even with only QD phonons.
(iii) The trap state interacts with vibrational modes of the ligand. This interaction, although intense,

renders only diagonal matrix elements because of the strong localization of both $\Psi_t(\mathbf{r})$ and the

vibrational mode. We have in mind mostly the stretching modes of both C-H and O-H groups. The
former is widely present in any organic capping and the latter is likely to be present owing to the
linking of the hydroxyl ions from the solvent to metal ions on the QD surface. The ligand
1-thioglycerol also contains 2 OH functional groups and the ligand MPA also has one OH functional
group (though in the latter case it is probably deprotonated in alkaline solution). Notice that the
presence of these ions is the only factor in the model that is influenced by the $H_2O \Leftrightarrow D_2O$
replacement, which strongly affects the non-radiative recombination lifetime, as our experimental
data show. Beyond the difference in the vibrational frequencies, and perhaps most importantly,
there is a five-fold difference in the dissociation constant value between the normal and heavy
water (larger for H_2O).[36]

With these three ingredients we can formulate a model that is supposed to describe the
essential physics involved in the renormalization of carrier's energy spectrum because of the
polaron effect including the non-adiabaticity. Two bare electron states will be considered, one (in
the QD core) optically active and the other (in the surface) dipole-forbidden. As we shall see, a
single surface state is sufficient to explain the main effect because the strong electron-phonon

---

[a] For strong confinement, $E_{1S} \ll V_0$, we have $kR \approx \pi$ and $\sin(kR) \approx \kappa/k = \sqrt{E_{1S}/(V_0 - E_{1S})}$. The

normalization constant is $A \approx (2\pi R)^{-1/2}$. For $a \ll R$ we replace the core wavefunction and the potential in Eq. (4)

by constants, $\Psi_t(R)$ and $\varphi_v(r = R, \vartheta = 0)$. The $(2l_p + 1)^{1/2}$ factor comes from the spherical harmonics'

normalisation.

interactions generate a manifold of polaron states. Let us note that a model invoking only one trap state (instead of postulating their distribution) was shown recently to be able to describe temperature dependent PL spectra in wider band gap QDs.[37] We shall neglect the small differences in frequencies of the different phonons confined in the dot and consider only one effective QD phonon mode ($\hbar\omega_1$) providing the non-diagonal interaction (i.e. the non-adibaticity) and only one ligand vibration mode ($\hbar\omega_0$) providing only the diagonal interaction with the surface state. The Hamiltonian has the form:

$$H = \sum_{i=1,2} E_i a_i^+ a_i + \sum_{\nu=0,1} \hbar\omega_\nu b_\nu^+ b_\nu + G_{12}\left(a_1^+ a_2 + a_2^+ a_1\right)\left(b_1^+ + b_1\right) + \sqrt{S}\,\hbar\omega_0\left(a_2^+ a_2 + a_2^+ a_2\right)\left(b_0^+ + b_0\right) \qquad (10)$$

Here $i = 1, 2$ denote the core and trap bare states, respectively, $a_i^+ (a_i)$ and $b_\nu^+ (b_\nu)$ are the creation (destruction) operators for electron and phonon, respectively, $G_{12} = \sum_\nu g_{12}^\nu$ and S is the Huang-Rhys parameter for the ligand mode. The latter is considered as a fitting parameter and its value is expected to be lower for the case of D_2O solvent because of the smaller number of vibrating hydroxyl groups present in the surface. We set the origin of the energy axis at the $1S_e$ level, so that $E_1 = 0$ and $E_2 = -\Delta$, and take $\hbar\omega_1 = 18\,\text{meV}$ (HgTe LO phonon energy) and $\hbar\omega_0 = 450\,\text{meV}$ as representative of the ligand stretching modes. The Hamiltonian (eq. 10) was diagonalized following the procedure proposed in Ref.[31], yielding the polaron eigenstates that are numerically exact. Using these, the SDS spectra were calculated by evaluating the trace of the electron Green's function.

As seen from the SDS spectrum presented in Fig. 6, there is a band of polaron states in the 1.0 – 1.2 eV range below the main absorption peak, which matches the hole ground state energy (marked by the arrow) and facilitates recombination with no phonons involved in this last step. If we assume that the electron thermalizes quickly enough and the probability distribution of its energy will be described by this SDS, which is non-zero at $E_{1S_{3/2}}$, the electron transfer from the polaron state to the valence band state becomes possible via elastic tunneling.[b] The probability of this process can be calculated by the Fermi's Golden Rule,

$$w_{t \to 1S_{3/2}} = \frac{2\pi}{\hbar}|T_{23}|^2 n\left(E_{1S_{3/2}}\right), \qquad (11)$$

---

[b] It is necessary to bear in mind that the polaron concept by itself does not yield thermalization or relaxation of the electron towards lower energies because polaron energy levels are *stationary* states of an electron coupled to discrete vibrational modes; it can provide only so-called pseudorelaxation, i.e. oscillatory dynamics involving different polaron states. Some additional interactions can be responsible for the true polaron relaxation. For instance, acoustic phonons can provide a small-scale energy dissipation necessary for its thermalization through the sufficiently dense energy spectrum created by the major electron-phonon interactions described by our effective Hamiltonian.[38]

where $n\left(E_{1S_{3/2}}\right)$ is the electron SDS at $E_{1S_{3/2}}$ (we shall label it as state 3 for clarity, while label 2 remains for the trap state) and T_{23} is the tunneling transition matrix element given by[39]:

$$T_{23} = \frac{\hbar^2}{2m} \int_{Su} \left[\Psi_2^*(\mathbf{r})\nabla\Psi_3(\mathbf{r}) - \Psi_3(\mathbf{r})\nabla\Psi_2^*(\mathbf{r})\right]d\mathbf{A}, \tag{12}$$

where the integral is taken over a surface that separates the trap and the QD core, which are considered disconnected while calculating (eq. 12). We choose the QD surface as Su and take $\Psi_3(\mathbf{r})$ in the same form as $\Psi_1(\mathbf{r})$ [eq. (6)] for simplicity, then the result (for $a << R$) is:

$$T_{23} = \sqrt{2\pi} \frac{\hbar^2}{2mR^2} \left(\frac{a}{R}\right)^{3/2} \frac{k}{\kappa} \left(1 + \frac{1}{2}\kappa R\right). \tag{13}$$

Taking for holes $m \approx 0.5m_0$, $kR \approx \pi$, $\kappa R \approx 10$, $R \approx 2$ nm and $R/a \approx 5$, we obtain $T_{23} \approx 10$ meV. With the spectral density of states $n\left(E_{1S_{3/2}}\right) \approx 10^{-7}$ meV^{-1} we have from (eq. 11) the tunneling probability of $w \approx 10^8$ s^{-1}. With the assumption of a much faster thermalization of the electron in accordance with the SDS shown in Fig. 6, this determines the recombination rate, τ_{nr}^{-1}. It is in qualitative agreement with the experimentally determined values exceeding 10^7 s^{-1} (see Fig. 4). Moreover, with the proposed model we are able to understand two effects seen in the experimental data (Fig. 5). First, the SDS within the polaron band slightly increases for smaller gap energies (longer wavelengths), as does the experimentally measured decay rate in Fig. 5 for both solvents. Secondly, the decay rate decreases in the whole spectral range studied when H_2O is replaced with D_2O. In terms of our model, it happens because there are less molecular vibration modes that contribute to the polaron effect, thus decreasing the effective diagonal coupling parameter.

Let us now turn to the resonant energy transfer channel. Its contribution is clearly seen in Fig. 5 as a dip in the spectrum of the experimentally measured PL lifetime for HgTe QDs in H_2O and also, to a lesser extent, in D_2O. The Guyot-Sionnest group proposed a Förster resonance energy transfer (FRET) mechanism for intraband relaxation,[40] later it was suggested as a possible non-radiative decay channel for colloidal QDs emitting in the near to mid IR region.[13, 41] In this model, the QD, an emitting dipole, transfers its electronic excitation energy to the surrounding (e.g. ligand shell) by resonantly coupling to its vibrational bands (combinations of C-H vibration modes). Essentially the same model was also considered in Ref.[42] where such a process was termed electronic-to-vibrational energy transfer (EVET). We shall also use this abbreviation for it is more specific than just FRET. The authors of Ref. 34 made numerical estimates of the EVET rate considering transfer to C-H vibration bands responsible for ligand absorption around 1200 nm. We can see such an absorption in Fig. 4, particularly for QDs dissolved in pure D_2O (so that virtually no O-H bonds could contribute). However, what is also important for QDs dissolved in H_2O is the EVET to the solvent molecules, as can be seen in Fig. 5. We can see a dip in τ_{avg} around 1000 nm, absent

for dots dissolved in D_2O, which correlates with the $2\nu_1 + \nu_3$ absorption band of water. Therefore both energy transfer channels need to be taken into account.

Using Fermi's Golden Rule, it is straightforward to derive the following expression for the transfer rate from the QD to a single molecule of solvent considered as a (randomly oriented) dipole located at a distance r:

$$w_{QD \to A} = \frac{4\pi\beta^2}{3\hbar\varepsilon_1^2 r^6} |d_{ex}|^2 |d_A|^2 \delta(\hbar\omega - E_A), \tag{14}$$

where $\varepsilon_1 = \mathrm{Re}\,\varepsilon$, ε is the (complex) dielectric constant of the solvent, $\hbar\omega = E_{1S_e} - E_{1S_{3/2}}$ is the exciton transition energy with the dipole moment matrix element d_{ex}, and E_A ($\mathbf{d}_A$) is the energy (transition dipole moment) of the molecular transition. The factor of (2/3) appears because of the average over different orientations of the dipoles and β^2 is the local field correction factor,

$$\beta = 3\varepsilon_1 / (2\varepsilon_1 + \varepsilon_{QD}^\infty),$$

where ε_{QD}^∞ is a background dielectric constant of the QD material.[c] Introducing the exciton transition oscillator strength, a dimensionless quantity defined as[43]

$$f_{osc} = \frac{2m_0\omega}{3e^2\hbar} |d_{ex}|^2,$$

and noting that

$$\frac{\pi}{3} |d_A|^2 \delta(\hbar\omega - E_A) = \mathrm{Im}\,\alpha_{\mathrm{mol}}(\omega),$$

where α_{mol} is the molecular polarizability of the solvent (or ligand) related to the considered vibrational mode, Eq. (14) can be conveniently rewritten as

$$w_{QD \to A} = \frac{6\beta^2 e^2}{m_0\omega\varepsilon_1^2 r^6} f_{osc}\, \mathrm{Im}\,\alpha_{\mathrm{mol}}(\omega). \tag{15}$$

The decay rate owing to EVET to the solvent is obtained by summing $w_{QD \to A}$ over all H_2O molecules,

---

[c] It is expressed as $\varepsilon_{QD} = \varepsilon_{QD}^\infty + 4\pi\chi$, where χ is the QD susceptibility related to the excitonic transitions and the background dielectric constant ε_{QD}^∞ takes into account all the electronic transitions excluding those considered explicitly in the susceptibility.

$$\gamma_{\text{EVET}}^{\text{solvent}} = 4\pi N \int\limits_{R^*}^{\infty} w_{QD \to A} r^2 dr$$

$$= \frac{2\beta^2 e^2}{m_0 \omega \varepsilon_1^2 R^{*3}} f_{osc} \operatorname{Im}\varepsilon(\omega),$$

(16)

where N is the number of molecules per unit volume. In the second line we have used the relation between the imaginary part of the solvent dielectric constant, $\operatorname{Im}\varepsilon$, and $\operatorname{Im}\alpha_{\text{mol}}$ following from the Clausius-Mossotti formula if the dispersion is small, $\operatorname{Im}\varepsilon \approx 4\pi N \operatorname{Im}\alpha_{\text{mol}}$. In Eq. (16) R^* is the radius of the QD plus the surrounding ligand layer thickness (i.e. its hydrodynamic radius). Although Eq. (15) is not valid for very large distances, we put the upper integration limit equal to infinity thanks to the fast convergence of the integral. Taking $\hbar\omega \approx 1\,\text{eV}$, $\varepsilon_1 \approx 2.2$, $\beta^2 \approx 0.13$ (for $\varepsilon_{QD}^{\infty} \approx 14$), $f_{osc} \approx 1.5$ (corresponding to the transition dipole moment of 20 D as in Ref. 34) and $R^* \approx 3\,\text{nm}$, we obtain $\gamma_{\text{EVET}} \approx 1.0 \times 10^{12}\,s^{-1} \times \operatorname{Im}\varepsilon(\omega)$. From the absorption coefficient of water (Ab) measured in Ref.[44], $Ab \approx 1\,\text{cm}^{-1}$ for $\lambda = 1.2\,\mu\text{m}$ (corresponding to the $\nu_1 + \nu_2 + \nu_3$ overtone), we obtain $\operatorname{Im}\varepsilon(\lambda = 1.2\,\mu\text{m}) = \lambda\sqrt{\varepsilon_1}/(2\pi) \times Ab \approx 3 \cdot 10^{-5}$ and $\gamma_{\text{EVET}}^{\text{solvent}} \approx 1.5 \cdot 10^7\,s^{-1}$ for the case of H_2O (and virtually zero for D_2O).

Similarly, for EVET to ligand molecules we have:

$$\gamma_{\text{EVET}}^{\text{ligand}} = 4\pi N \int\limits_{R}^{R^*} w_{QD \to A} r^2 dr$$

$$= \frac{2\beta^2 e^2}{m_0 \omega \varepsilon_{lig}'^2 R^{*3}} \left[\left(\frac{R^*}{R}\right)^3 - 1 \right] f_{osc} \operatorname{Im}\varepsilon_{lig}(\omega),$$

(17)

where ε_{lig} is the ligand's dielectric constant and $\varepsilon_{lig}' \approx \varepsilon_{lig}$ is its real part. From the absorption spectra presented in Fig. 5 we can estimate $\left(\operatorname{Im}\varepsilon_{lig}/\operatorname{Im}\varepsilon_{H_2O}\right)\big|_{1200\,\text{nm}} \approx 0.3$. Taking $R^*/R \approx 1.5$ we obtain $\gamma_{\text{EVET}}^{\text{ligand}} \approx 0.7\gamma_{\text{EVET}}^{H_2O}$ in the vicinity of $\lambda \approx 1200\,\text{nm}$ where these two channels act in parallel in the case of H_2O and only the ligand channel is present for D_2O. These estimates are in excellent

agreement with the experimental data shown in Fig. 5.[d]

Radiative decay rate

The radiative decay rate of an emitting dipole is given by[43]

$$\gamma_r = \frac{4\pi^2 |\mathbf{d}|^2 \omega}{3\hbar \varepsilon_1(\omega)} \rho(\omega),\tag{17}$$

where $\rho(\omega)$ is the photon density of states (PDS). If the emitting dipole is a spherical QD, the right-hand side of eq. (17) has to be multiplied by the factor β^2 taking into account the depolarization effects. Generally speaking, a change of γ_r can be caused by one of the following:

    i.   Change of the transition matrix element (dipole moment $\mathbf{d}$).
    ii.   Variation of the PDS; an example of this is the Purcell effect[46] where the emission probability in a microcavity depends very strongly on the detuning between the emission mode and the microcavity resonance mode.

We exclude the variation of the dielectric constant as a direct factor that could change eq. (17) because, as we saw above, the imaginary part of solvent dielectric constant is of the order of 10^{-5} and so is the order of magnitude of the variation of the real part (ε_1) due to the H_2O/D_2O replacement. However, it does not immediately exclude the possibility that the PDS is modified with respect to its usual parabolic shape in vacuum, $\rho_0 = \omega^2/\pi^2 c^3$ (c is the velocity of light), because of the solvent dielectric constant dispersion. It can be shown that for a homogeneous dispersive medium where $\varepsilon_1 \equiv \mathrm{Re}\,\varepsilon(\omega) \gg \mathrm{Im}\,\varepsilon(\omega)$ the PDS is given by

$$\rho(\omega) = \frac{\omega^2}{\pi^2 c^3}\left[\varepsilon_1(\omega) + \frac{\omega}{2}\left(\frac{d\varepsilon_1(\omega)}{d\omega}\right)\right]\sqrt{\varepsilon_1(\omega)}.\tag{18}$$

If $\varepsilon_1(\omega)$ changes rapidly with ω (near a resonance), the derivative term in eq. (18) can become large. We would like to emphasize that this is not an absorption effect, the latter is much weaker. Indeed, we can estimate the relative importance of the dispersion and absorption effects (for a single resonance) as follows:

---

[d] Lhuillier et al.[45] estimated $f_{osc} \approx 5-10$ for HgTe QDs of the size range considered here, which yields about 5 times higher γ_{EVET}. The obtained agreement with experiment in terms of EVET rates suggests that the oscillator strength in our HgTe QDs is indeed of the order of unity.

$$\frac{\omega}{2}\left(\frac{d\varepsilon_1(\omega)}{d\omega}\right)\bigg/\mathrm{Im}\,\varepsilon(\omega) \approx \frac{\omega_0}{2\Gamma} \gg 1,$$

where ω_0 and Γ are the resonance frequency and damping, respectively. With the parameters extracted from the measured absorption coefficient we found that the dispersion-related variations of the PDS, $\left\{\rho(\omega)\big/\left[\varepsilon_1^{3/2}\rho_0(\omega)\right]-1\right\}$, are of the order of $2\cdot10^{-4}$ in the relevant spectral range. It means that this effect cannot explain the observed changes of the radiative lifetime and we are left with the only possibility that the matrix element of the dipole-allowed optical transition inside the QD core is sensitive to the QD environment. However, it would contradict the observed invariance of the absorption spectrum with respect to the solvent replacement if the absorbing and emitting states in the QDs are the same.

One possibility to explain this puzzling situation is to admit that the solvent replacement affects those processes which we assumed to be very fast, namely, the hot carrier relaxation into the ground exciton state and/or thermalization of the trapped electron through the polaron spectrum, are not much faster than the emission and the recombination via elastic tunneling, respectively. The rates of these processes (excluded from our model) may depend on the vibrational degrees of freedom of the QD environment and therefore be affected by the solvent replacement. Then the population of the emitting states will not be entirely determined by the temperature (as assumed in our model, see Supplementary Material) and will depend also on the QD environment.

Conclusions

We have compared the radiative and non-radiative recombination rates in aqueous solutions of HgTe and CdTe QDs in an effort to establish the mechanisms of the influence from the ligand and solvent environment close to the surface of the dots. By transferring the same QD samples between H_2O and D_2O solvents and also by exchanging solvents and ligands to transfer from aqueous to organic systems, we collected extensive spectroscopic data on the PL QYs and PL decay times. From their analysis we have been able to gain insight into the relative importance of the resonant energy transfer to the solvent and ligand molecules (EVET) and the simultaneously present non-resonant channel of carrier recombination in HgTe dots. The latter involves several processes, namely, (i) coupling of the QD core state to a surface trap state, mediated by a broad variety of QD optical phonons with non-zero angular momenta, (ii) formation of a dense polaron spectrum caused by the strong interaction between the trap state and vibrational modes of the QD environment in combination with the non-adiabatic effect of (i), and (iii) thermalization of one of the carriers through this staircase of polaron energy levels and finally recombination with the partner particle via an elastic tunneling process. The process (ii) involves some IR overtone and combination bands of the ligand and the water solvent, so when some of these modes are removed from the relevant spectral range by the H_2O to D_2O replacement, the non-radiative lifetime increases. From our results it follows that this channel is superior to EVET in importance and operates in a broad energy range, while the latter is efficient only within narrow bands around the vibration mode frequencies. This

understanding is important for further development of IR QDs for emissive devices where the challenge is to make non-radiative recombination slow.

Maximization of the oscillator strength for radiative recombination by ensuring strong overlap of the electron and hole wavefunctions in the QDs is a must for emissive materials, but the converse may help the efficiency of photovoltaics where CdTe is an important material. Interestingly, we found virtually no solvent influence upon the radiative lifetime in CdTe QDs, while the effective non-radiative lifetime seems to increase by a factor of 1.6 compared to H_2O. The solvent exchange ($H_2O \rightarrow D_2O$) is found to increase the overall quantum yield of CdTe QD samples by about 10%, probably by increasing the fraction of bright QDs (those which are free from surface traps) in the ensemble, which can be the main cause of the above mentioned effect. For CdTe QDs surface traps are considered to be responsible for the major non-radiative recombination mechanism in the literature,[9,10,47] although the participation of phonons and/or molecular vibrations in such processes is always indispensable.[12, 25, 36] We have shown that the existence of a single surface trap state strongly coupled to molecular vibrations of the ligand allows for explaining our experimental data quantitatively. Moreover, our findings suggest that the polaron-trap-based recombination channel proposed here for HgTe QDs, similar in physics to the relaxation mechanism in wider bandgap dots such as CdSe,[12] is more efficient than the resonant energy transfer (EVET) channels to either solvent or ligand.

Acknowledgements

References

1.   M. Chen; H. Yu; S. V. Kershaw; H. Xu; S. Gupta; F. Hetsch; A. L. Rogach; N. Zhao, *Advanced Functional Materials* 2014, 24, 53-59.

2.   C. H. M. Chuang; P. R. Brown; V. Bulovic; M. G. Bawendi, *Nature Materials* 2014, 13, 796-801.

3.   J. J. Choi; W. N. Wenger; R. S. Hoffman; Y. F. Lim; J. Luria; J. Jasieniak; J. A. Marohn; T. Hanrath, *Adv Mater* 2011, 23, 3144-3148.

4.   B. N. Pal; Y. Ghosh; S. Brovelli; R. Laocharoensuk; V. I. Klimov; J. A. Hollingsworth; H. Htoon, *Nano Letters* 2011, 12, 331-336.

5.   A. L. Rogach; T. Franzl; T. A. Klar; J. Feldmann; N. Gaponik; V. Lesnyak; A. Shavel; A. Eychmüller; Y. P. Rakovich; J. F. Donegan, *The Journal of Physical Chemistry C* 2007, 111, 14628-14637.

6.   C. Sun; Y. Zhang; Y. Wang; W. Y. Liu; S. Kalytchuk; S. V. Kershaw; T. Q. Zhang; X. Y. Zhang; J. Zhao; W. W. Yu; A. L. Rogach, *Applied Physics Letters* 2014, 104, 261106.

7. G. Allan; C. Delerue, *Phys. Rev. B* 2012, 86, 165437.

8. S. E. Keuleyan; P. Guyott-Sionnest; C. Delerue; G. Allan, *ACS Nano* 2014, 8, 8676-8682.

9.   B. Omogo; J. F. Aldana; C. D. Heyes, *Journal of Physical Chemistry C* 2013, 117, 2317-2327.

10. M. Califano, *ACS Nano* 2015, 9, 2960-2967.

11. H. Chung; H. Choi; D. Kim; S. Jeong; J. Kim, *The Journal of Physical Chemistry C* 2015, 119, 7517-7524.

12. P. Kambhampati, *The Journal of Physical Chemistry C* 2011, 115, 22089-22109.

13. S. Keuleyan; J. Kohler; P. Guyot-Sionnest, *The Journal of Physical Chemistry C* 2014, 118, 2749-2753.

14. S. L. Wu; J. Dou; J. Zhang; S. F. Zhang, *Journal of Materials Chemistry* 2012, 22, 14573-14578.

15. S. V. Kershaw; S. Kalytchuk; O. Zhovtiuk; Q. Shen; T. Oshima; W. Yindeesuk; T. Toyoda; A. L. Rogach, *Physical Chemistry Chemical Physics* 2014, 16, 25710-25722.

16. S. V. Kershaw; A. L. Rogach, *Zeitschrift für Physikalische Chemie* 2015, 229, 23-64.

17. A. Rogach; S. V. Kershaw; M. Burt; M. T. Harrison; A. Kornowski; A. Eychmüller; H. Weller, *Advanced Materials* 1999, 11, 552-555.

18. A. Al-Otaify; S. V. Kershaw; S. Gupta; A. L. Rogach; G. Allan; C. Delerue; D. J. Binks, *Physical Chemistry Chemical Physics* 2013, 15, 16864-16873.

19. S. E. Lappi; B. Smith; S. Franzen, *Spectrochimica Acta Part a-Molecular and Biomolecular Spectroscopy* 2004, 60, 2611-2619.

20. H. Sato; M. Tachiya, *J. Chem. Phys.* 1981, 75, 2870.

21. Y. Ebenstein; T. Mokari; U. Banin, *Appl. Phys. Lett.* 2002, 80, 4033.

22. J. Yao; D. R. Larson; H. D. Vishwasrao; W. R. Zipfel; W. W. Webb, *PNAS* 2005, 102, 14284.

23. N. Durisic; A. G. Godin; D. Walters; P. Grütter; P. W. Wiseman; C. D. Heyes, *ACS Nano* 2011, 5, 9062.

24. C. de Mello Donega, R. Koole, *J. Phys. Chem. C* 2009, 113, 6511.

25. J. S. Kamal, A. Omari, K. Van Hoecke, Q. Zhao, A. Vantomme, F. Vanhaecke, R. K. Capek, Z. Hens. *Phys. Chem. C* 2012, 116, 5049.

26. G. D. Mahan, *Many-Particle Physics*. Springer US: Boston, MA, 2000.

27. J. Mooney; M. M. Krause; J. I. Saari; P. Kambhampati, *The Journal of Chemical Physics* 2013, 138, 204705.

28. M. Hamma; R. P. Miranda; M. I. Vasilevskiy; I. Zorkani, *Journal of Physics: Condensed Matter* 2007, 19, 346215.

29. E. A. Silinsh; A. Klimkāns; S. Larsson; V. Čápek, *Chemical Physics* 1995, 198, 311-331.

30. R. C. Cooney; S. L. Sewall; K. E. H. Anderson; E. A. Dias, P. Kambhampati, *Phys. Rev. Lett*. 2007, 98, 177403.

31. M. I. Vasilevskiy; E. V. Anda; S. S. Makler, *Physical Review B* 2004, 70, 035318.

32. M. I. Vasilevskiy; A. G. Rolo; M. V. Artemyev; S. A. Filonovich; M. J. M. Gomes; Y. P. Rakovich, *physica status solidi (b)* 2001, 224, 599-604.

33. V. Dzhagan; M. Y. Valakh; J. Kolny-Olesiak; I. Lokteva; D. R. T. Zahn, *Applied Physics Letters* 2009, 94, 243101.

34. V. M. Fomin; V. N. Gladilin; J. T. Devreese; E. P. Pokatilov; S. N. Balaban; S. N. Klimin, *Physical Review B* 1998, 57, 2415-2425.

35. R. P. Miranda; M. I. Vasilevskiy; C. Trallero-Giner, *Physical Review B* 2006, 74, 115317.

36. N. N. Greenwood; A. Earnshaw, *Chemistry of the elements*. 2nd ed.; Butterworth-Heinemann: Oxford, 1997.

37. J. Mooney; M. M. Krause; J. I. Saari; P. Kambhampati, *Phys. Rev. B* 2007, 87, 081201(R).

38. T. Stauber; M. I. Vasilevskiy, *Physical Review B* 2009, 79, 113301.

39. J. Bardeen, *Physical Review Letters* 1961, 6, 57-59.

40. P. Guyot-Sionnest, B. Wehrenberg, and D. Yu, *J. Chem. Phys. 2005, 123, 074709.*

41. A. Pandey; P. Guyot-Sionnest, *Science* 2008, 322, 929-932.

42. A. Aharoni; D. Oron; U. Banin; E. Rabani; J. Jortner, *Physical Review Letters* 2008, 100, 057404.

43. L. Novotny; B. Hecht, *Principles of Nano-Optics*. Cambridge University Press: 2012.

44. J. A. Curcio; C. C. Petty, *J. Opt. Soc. Am.* 1951, 41, 302-302.

45. E. Lhuillier; S. Keuleyan; P. Guyot-Sionnest, *Nanotechnology* 2012, 23, 175705.

46. E. M. Purcell; H. C. Torrey; R. V. Pound, *Physical Review* 1946, 69, 37-38.

47. A. M. Kapitonov; A. P. Stupak; S. V. Gaponenko; E. P. Petrov; A. L. Rogach; A. Eychmüller, *The Journal of Physical Chemistry B* 1999, 103, 10109-10113.